

Demonstration of High-Throughput Intra-Datacenter Switches Using Interleaved AWGs for Nyquist WDM

Takuma Kuno¹, Takumi Mitsuya¹, Yojiro Mori¹, Hiroshi Hasegawa¹, Ken-ichi Sato²

¹Nagoya University, Furo-cho, Chikusa, Nagoya, 464-8603 Japan

²The National Institute of Advanced Industrial Science and Technology (AIST), 1-1-1 Umezono, Tsukuba, Ibaraki, 305-8568 Japan
kuno.takuma@j.mbox.nagoya-u.ac.jp

Abstract: We demonstrate a high-throughput optical circuit switch for intra-datacenter networks. DP-32QAM and Nyquist WDM are used to enhance the spectral efficiency of the switch. Experiments show the total switch throughput of 8.512 Pbps. © 2022 The Authors

1. Introduction

Intra-datacenter traffic is exploding due to the spread of cloud-computing services and video-streaming services. The total amount of intra-datacenter traffic is about five times that of IP traffic. Current datacenters employ electrical switches to connect top-of-rack switches even though the transmission link adopts optical fibers [1]. Such an architecture creates excessive power consumption owing to the large number of optical-to-electrical and electrical-to-optical conversions demanded by the electrical switching. In order to solve this problem, optical and electrical hybrid switch network architectures and fully optical switch network architectures are being extensively studied [2-5]. These approaches can reduce the power consumption of datacenter networks by replacing the electrical switches with optical circuit switches.

To process a large amount of intra-datacenter traffic cost-effectively, optical circuit switches must have high throughput. So far, many types of optical circuit switch architectures are being intensively studied [6-12]. Among them, the combination of delivery-and-coupling (DC) space switches and wavelength-routing (WR) switches based on arrayed-waveguide gratings (AWGs) is a promising candidate for intra-datacenter interconnection [11,12]. With this switch architecture, we experimentally demonstrated the switch throughput of 2.1 Pbps, where 32 Gbaud DP-16QAM signals aligned on a 50 GHz grid were used to realize WR switching [11]. To increase the switch throughput further, spectrum efficiency of the WR switch part must be enhanced. The use of Nyquist wavelength-division multiplexing (WDM) is attractive because it can enhance spectrum efficiency by minimizing the guardband width. However, the filter slope of AWGs used for WR switching is too gradual to route Nyquist-WDM signals.

In this paper, we demonstrate a high-throughput optical circuit switch based on Nyquist WDM for the first time. The introduction of Nyquist WDM is enabled by a pair of AWGs whose passbands are interleaved. The feasibility of the proposed switch is confirmed by experiments using 95-wavelength 2.8 Tbps signals comprising 2 wavelength sub-channels and 7 spatial sub-channels, where each sub-channel consists of 24 Gbaud DP-32QAM signals accommodated within 25 GHz bandwidth. By using 32-port DC space switches to connect these WR switches, the total switch throughput reaches 8.512 Pbps ($95 \times 2.8 \text{ Tbps} \times 32$).

2. Proposed switch architecture

2.1. Basic structure

Figure 1 shows the basic switch architecture [11,12]; it combines DC space switches and WR switches. The switch consists of MN wavelength-tunable transmitters supporting N wavelengths and L spatial sub-channels, $LM \times M$ DC space switches comprising M $1 \times M$ optical selectors and $M \times 1$ optical couplers, $LM \times N$ WR switches that exploit AWGs, and MN wavelength-fixed receivers supporting L spatial sub-channels, where N represents the number of wavelengths and M denotes the port count of the DC switch.

The switching operation is as follows: L spatial sub-channel signals are generated by a transmitter supporting N wavelengths, where the wavelength is assigned according to the target output port. The L spatial sub-channel signals are then input to L single-core fibers or an L -core fiber. After transmission, the L spatial sub-channel signals are jointly directed by $L \times M \times M$ DC space switches and sent to L WR switch parts. In each space layer, multiple wavelength signals are demultiplexed by an $N \times N$ WR switch comprising an optical coupler and AWGs. Finally, the target signal comprising L spatial sub-channels is detected by the target receiver. It should be noted that the skews among spatial sub-channels can be easily offset by digital buffers in the receiver; no complicated MIMO processing is necessary since we do not consider the use of coupled-core fibers or multi-mode fibers. This switch configuration also obviates the use of immature SDM devices, e.g., multicore erbium-doped fiber amplifiers (EDFAs). In addition,

DC space switches and WR switches can be compactly implemented with planar-lightwave-circuit technologies or silicon-photonics technologies [12-14]. With spatial sub-channels, the switch throughput can be increased while keeping the cost per bit because L spatial sub-channels can be switched by parallelized optical sub-switches.

2.2. Switch throughput enhancement with Nyquist WDM technique

The switch throughput is given by $SMBE$, where S , M , B , and E denote the number of spatial sub-channels, the DC space switch port count, the available bandwidth of WR switches, and spectrum efficiency of WR switches, respectively. To increase the switch throughput further, these four design parameters need to be increased. However, the number of spatial sub-channels, S , is limited by the number of available cores in a cable. Expansion of the DC space switch port count, M , is infeasible because the insertion loss of the DC space switch increases with its port count. The available bandwidth of WR switches, B , is limited by the available bandwidth of optical devices such as tunable lasers, EDFAs, and AWGs. Thus, enhancement of spectrum efficiency, E , is needed to increase the switch throughput. Therefore, the use of Nyquist WDM technique is attractive. However, Nyquist-WDM signals cannot be demultiplexed with AWGs because the filter slope is too gradual.

To alleviate the spectrum narrowing due to AWGs, we exploit a pair of AWGs whose passbands are interleaved. Figure 2 shows the proposed WR switch that utilizes Nyquist WDM, where a 6×6 WR switch is used as an example. The WR switch consists of n $N/n \times 1$ optical couplers, n EDFAs, n 1×2 splitters, and a pair of $n \times N/2$ uniform-loss and cyclic frequency (ULCF) AWGs [12]. Note that multiple wavelength sub-channels can be bundled as one channel to match the signal bandwidth and the passband bandwidth of AWGs. Routing operation of the switch consists of four steps: first, N wavelength signals are aggregated at n $N/n \times 1$ optical couplers; next, aggregated signals are amplified by an EDFA; after that, signals are branched by 1×2 splitters; finally, N wavelength signals are demultiplexed by a pair of $n \times N/2$ ULCF AWGs. Because each ULCF AWG is designed for only odd- or even-number channels, the passband is doubled compared to that of a single AWG. Although parts of signals adjacent to the target signal still exist after a WR switch, the following coherent receiver eliminates them with analog and digital filters.

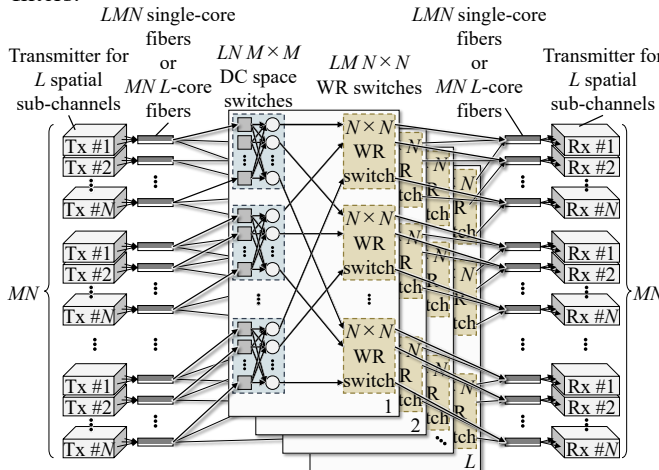


Fig. 1. Basic switch architecture using DC space switches and WR switches.

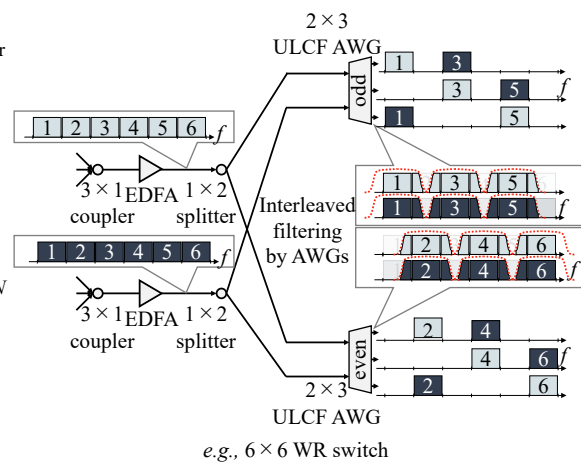


Fig. 2. Routing operation of the proposed WR switch.

3. Experiments

We conducted experiments to evaluate the performance of our optical switch architecture. Figure 3 shows the experimental setup. At the transmitter side, a continuous wave (CW) was generated by a tunable laser. A 24 Gbaud 32QAM signal was created by a lithium-niobate IQ modulator driven by an arbitrary-waveform generator. Next, a dual-polarization signal was created by a polarization-division multiplexing (PDM) emulator consisting of polarization-beam splitter, a 10-ns-delay fiber, and a polarization-beam combiner (PBC). The adjacent-wavelength signals were created in the same manner. After the signal power was controlled by an EDFA and a variable optical attenuator (VOA), the signals were split by a 1×8 splitter. Here, seven of the tributaries were input to a 2-km 7-core fiber. Power of each signal was set to 7 dBm. The loss of the 7-core fiber was 4 dB; this included the fan-in and fan-out losses. After passing through the 7-core fiber, the target signal was input to the switch under the test. Here, we constructed part of a 3040×3040 optical circuit switch, where DC-switch scale M was 32. The measured losses of the 1×8 optical coupler and the DC space switch part were 9.8 dB and 18.4 dB, respectively. We used a WR switch configuration that combined 12 1×2 splitters and a pair of 12×48 ULCF AWGs; each ULCF AWG was fabricated

with PLC technologies [12]; the passband spacing was designed for 100 GHz grid systems. Figure 4(a) and (b) show the chip and module box of the ULCF AWGs, respectively; their dimensions were $50 \times 50 \text{ mm}^2$ and $70 \times 90 \text{ mm}^2$, respectively. As inter-band crosstalk, 187 non-target signals with different wavelengths were combined with the target signal with its adjacent signals via an 8×1 aggregation coupler, *i.e.*, 190 wavelengths in total. We took the 190-wavelength 200 Gbps signals to be 95-wavelength 400 Gbps dual-carrier signals. Additionally, 11 signals were input to the remaining input ports of a ULCF AWG as intra-band crosstalk; their wavelength matched that of the target signal. The extinction ratio of the ULCF AWG ranged from 32 dB to 39 dB depending on signal wavelength and input/output port. Finally, the target signal was detected by a digital coherent receiver.

Fig. 5 shows the constellation map of the received DP-32QAM signal and measured BERs on a sub-channel basis. We evaluated signals from the center core in the 7-core fiber to consider the worst condition in terms of inter-core crosstalk. Symbol states of the received signal are clearly separated. We confirmed that all BERs achieved the target value of 10^{-2} . The overall throughput is 8.512 Tbps ($=95 \times 2.8 \text{ Tbps} \times 32$).

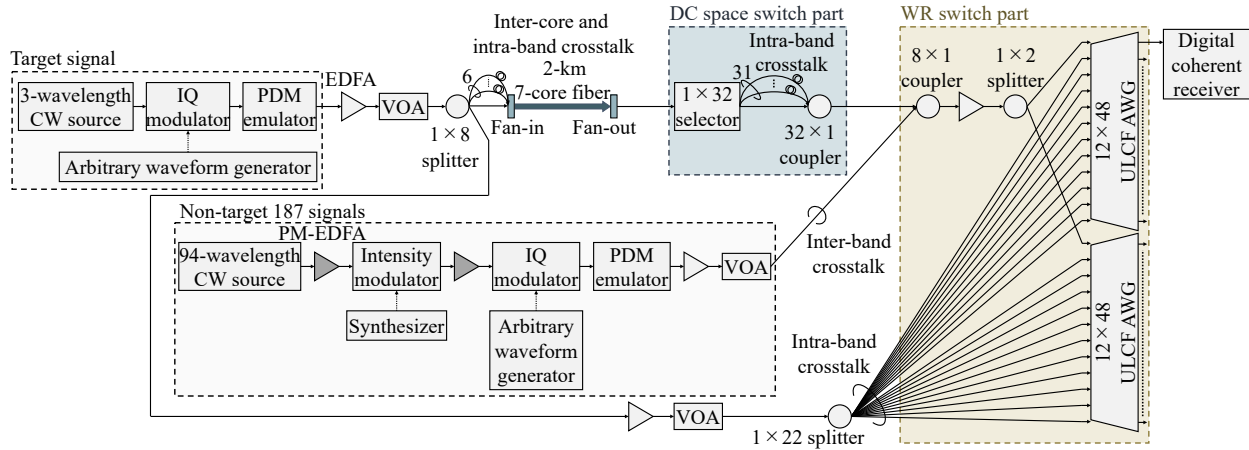


Fig. 3. Experimental setup.

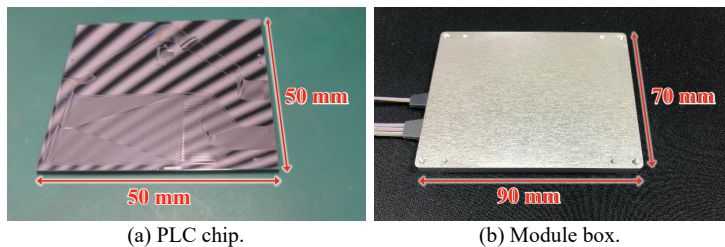


Fig. 4. The tested 12×48 ULCF AWG fabricated with PLC technologies.

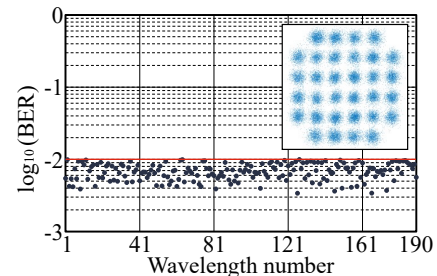


Fig. 5. The constellation map of received signals and 190 BERs measured at 95 ports.

4. Conclusion

We confirmed the feasibility of the proposed optical circuit switch that employs Nyquist WDM. This is enabled by pairs of AWGs whose passbands are interleaved. We measured the BERs of 2.8 Tbps DP-32QAM signals comprising 2 wavelength sub-channels and 7 spatial sub-channels, where each sub-channel is a 24 Gbaud DP-32QAM signal assigned in 25 GHz bandwidth. The total throughput reached 8.512 Pbps, and the total switch port count was 3040×3040 .

Acknowledgment: This paper is based on results obtained from a project (JPNP16007) commissioned by the New Energy and Industrial Technology Development Organization (NEDO).

5. References

- [1] C. Kachris *et al.*, Optical Interconnects for Future Data Center Networks (Springer, 2012).
- [2] X. Xue *et al.*, OFC, W1F.5 (2020).
- [3] F. Yan *et al.*, IEEE/OSA J. Opt. Commun. Netw. **10**, 1-14 (2018).
- [4] K. Sato *et al.*, IEEE Commun. Mag. **51**, 46-52 (2013).
- [5] C. Kachris *et al.*, IEEE Commun. Surv. **14**, 1021-1036 (2012).
- [6] K. Tanizawa *et al.*, ECOC, Th.1.A (2019).
- [7] T. J. Seok *et al.*, OSA Optica **6**, 490-494 (2019).
- [8] Q. Cheng *et al.*, OSA Photonics Res. **7**, 155-161 (2019).
- [9] K. Suzuki *et al.*, IEEE/OSA J. Lightw. Technol. **37**, 116-122 (2018).
- [10] M. Ding *et al.*, IEEE J. Sel. Top. Quantum Electron. **24**, 1-8 (2017).
- [11] E. Honda *et al.*, OFC, W1F.2 (2020).
- [12] H. Nagai *et al.*, IEEE/OSA J. Opt. Commun. Netw. **10**, 82-89 (2018).
- [13] S. Nakamura *et al.*, IEEE J. Sel. Top. Quantum Electron. **22**, 185-193 (2016).
- [14] W. Bogaerts *et al.*, IEEE J. Sel. Top. Quantum Electron. **16**, 33-44 (2010).